Self-Assembly of Recombinant Prion Protein of 106 Residues†

Ilia V. Baskakov,[‡,§] Claus Aagaard,[‡,§] Ingrid Mehlhorn,[‡,§] Holger Wille,[‡,§] Darlene Groth,[‡,§] Michael A. Baldwin,[‡,§,||] Stanley B. Prusiner,[‡,§,⊥] and Fred E. Cohen*[,⊥,@,#]

Institute for Neurodegenerative Diseases, Department of Neurology, Department of Biochemistry and Biophysics, Department of Cellular and Molecular Pharmacology, Department of Medicine, and Department of Pharmaceutical Chemistry, University of California, San Francisco, California 94143

Received October 7, 1999; Revised Manuscript Received December 27, 1999

ABSTRACT: The central event in the pathogenesis of prion diseases is a profound conformational change of the prion protein (PrP) from an α-helical (PrP^C) to a β-sheet-rich isoform (PrP^{Sc}). The elucidation of the mechanism of conformational transition has been complicated by the challenge of collecting high-resolution biophysical data on the relatively insoluble aggregation-prone PrP^{Sc} isoform. In an attempt to facilitate the structural analysis of PrP^{Sc}, a redacted chimeric mouse-hamster PrP of 106 amino acids (MHM2 PrP106) with two deletions (Δ23−88 and Δ141−176) was expressed and purified from *Escherichia coli*. PrP106 retains the ability to support PrP^{Sc} formation in transgenic mice, implying that it contains all regions of PrP that are necessary for the conformational transition into the pathogenic isoform [Supattapone, S., et al. (1999) *Cell 96*, 869−878]. Unstructured at low concentrations, recombinant unglycosylated PrP106 (rPrP106) undergoes a concentration-dependent conformational transition to a β-sheet-rich form. Following the conformational transition, rPrP106 possesses properties similar to those of PrP^{Sc}106, such as high β-sheet content, defined tertiary structure, resistance to limited digestion by proteinase K, and high thermodynamic stability. In GdnHCl-induced denaturation studies, a single cooperative conformational transition between the unstructured monomer and the assembled β-oligomer was observed. After proteinase K digestion, the oligomers retain an intact core with unusually high β-sheet content (>80%). Using mass spectrometry, we discovered that the region of residues 134−215 of rPrP106 is protected from proteinase K digestion and possesses a solvent-independent propensity to adopt a β-sheet-rich conformation. In contrast to the PrP^{Sc}106 purified from the brains of neurologically impaired animals, multimeric β-rPrP106 remains soluble, providing opportunities for detailed structural studies.

Prions cause a variety of degenerative neurologic diseases that can be infectious, inherited, or sporadic in origin (*2*). A key event in all three forms of prion diseases is the replication of the pathological isoform of the prion protein (PrP^{Sc}),[1] which exhibits substantial β-sheet structure and partial proteinase K resistance, from the predominantly α-helical, proteinase-sensitive isoform (PrP^C) (*3*). Despite advances in understanding the molecular basis of prion diseases, the mechanism of propagation remains poorly understood.

Elucidation of the structure of both PrP isoforms is fundamental to understanding the molecular mechanisms of the conformational transition from the α-helical form to the β-sheet form. In vivo, PrP^C is a GPI-anchored glycoprotein with two N-linked sugars and a disulfide bridge; PrP appears to bind copper through histidine residues with a 4:1 stoichiometry (*2*, *4*). The NMR structure of recombinant rPrPs and their fragments folded into an α-helical conformation has been determined in the absence of copper. Some of these rPrP structures are thought to resemble PrP^C (*5*−*8*). Structural information about the PrP^{Sc} isoform is much more limited. Upon purification, PrP^{Sc} tends to aggregate into insoluble multimers (*9*). Using proteinase K digestion, the core of PrP^{Sc} resistant to digestion (residues 90−231), designated PrP 27−30, was identified (*10*, *11*). PrP 27−30 is assembled into β-sheet-rich fibrils with the properties of amyloid (*12*). Several studies using FTIR have been reported for PrP^{Sc}, PrP 27−30, and PrP^{Sc}106 as well as the proposal of a structural model for PrP^{Sc} (*13*), but no three-dimensional structural information is available at atomic resolution. Fibrillogenic PrP peptide fragments have been studied by solid-state NMR and fiber diffraction (*14*−*16*). Although a few studies have demonstrated the ability to fold recombinant

† This work was supported by grants from the National Institutes of Health (NS14069, AG08967, AG02132, and AG10770) and a gift from the Leila and Harold Mathers Foundation. Mass spectrometry was supported by NIH Grant NCRRBRTP RR01614. I.V.B. is supported by the French Foundation for Alzheimer's Research.

* To whom correspondence should be addressed: Department of Cellular and Molecular Pharmacology, Box 0450, University of California, San Francisco, CA 94143-0450. Telephone: (415) 476-8519. Fax: (415) 476-6515. E-mail: cohen@cmpharm.ucsf.edu.

‡ Institute for Neurodegenerative Diseases.

§ Department of Neurology.

|| Department of Pharmaceutical Chemistry.

⊥ Department of Biochemistry and Biophysics.

@ Department of Cellular and Molecular Pharmacology.

Department of Medicine.

[1] Abbreviations: PrP^C, normal isoform of prion protein; PrP^{Sc}, scrapie-associated isoform of prion protein; PrP 27−30, proteinase K-resistant core of PrP^{Sc}; PrP106, prion protein of 106 residues; PrP^{Sc}106, scrapie-associated isoform of prion protein of 106 residues; rPrP106, recombinant prion protein of 106 residues; GPI, glycophosphoinositol; GdnHCl, guanidinium hydrochloride; SEC, size-exclusion chromatography; MS, mass spectrometry; ESIMS, electrospray ionization mass spectrometry; TFE, trifluoroethanol; CD, circular dichroism; PMSF, phenylmethanesulfonyl fluoride.

10.1021/bi9923353 CCC: $19.00
Published on Web 02/19/2000

PrP to the β-sheet-rich conformation, no infectious isoform of protein has been created in vitro de novo (*17*, *18*). Thus, the difficulties associated with the structural studies of PrP^{Sc} together with long incubation times for assays of infectivity create a challenge.

In an effort to understand the mechanism of PrP^{Sc} formation, we sought to identify PrP fragments that can support prion infectivity as measured by bioassay. Recently, we demonstrated that 50% of the PrP residues may be removed, while the remaining polypeptide supports PrP^{Sc} propagation in transgenic mice that develop neuropathologic changes characteristic of scrapie (*1*). The resulting mini-prion is composed of redacted chimeric mouse-hamster MHM2 PrP^{Sc}106, which consists of 106 amino acids with two substantial deletions. The N-terminal deletion (Δ23−88) removes most of the octarepeat regions (*4*, *19*−*21*), whereas the deletion of residues 141−176 removes the regions that in PrP^{C} form helix A and one of the short β-strands (*5*−*8*). To our knowledge, PrP106 is the shortest polypeptide chain currently known that retains the ability to support PrP^{Sc} formation in vivo (*1*). To gain a better understanding of the properties of PrP106, we expressed, purified, and biophysically characterized recombinant PrP106 (rPrP106).

rPrP106 was found to be unstructured at sub-micromolar concentrations, whereas it underwent a concentration-dependent conformational transition at micromolar concentrations, adopting a β-sheet-rich conformation. The formation of the β-sheet-rich conformation is accompanied by cooperative self-assembly to ordered oligomers with defined tertiary structure. Using size-exclusion chromatography, we demonstrated that only two thermodynamic ensembles, the unfolded monomer and the β-sheet-rich oligomer, are populated under equilibrium GdnHCl-induced denaturation. The assembled oligomer of the recombinant protein possesses some physical properties similar to those of PrP^{Sc} extracted from the brains of sick animals, such as partial resistance to digestion by proteinase K and high β-sheet content. In contrast to PrP^{Sc}106, rPrP106 remains soluble in aqueous solution upon oligomerization, thereby providing opportunities for more detailed structural studies. Following proteinase K digestion of the assembled oligomers, the proteinase K-resistant core contains an unusually high amount of β-sheet structure (>80%). Using mass spectrometry, we have identified the region of rPrP106 that is protected from proteinase K digestion and possesses a solvent-independent propensity to adopt β-sheet conformation.

MATERIALS AND METHODS

Cloning, Expression, and Purification of Recombinant PrP MHM2(106). The MHM2(106) PrP gene was amplified from a eukaryotic expression construct (*22*) by PCR (Perkin-Elmer) using a 5′-oligonucleotide with a *Mlu*I restriction site within the coding sequence of the STII signal peptide (*23*, *24*), a 3′-oligonucleotide with a TGA stop codon, and a *Bam*HI restriction site incorporated (*25*). The amplified product was digested with *Mlu*I−*Bam*HI, purified and ligated into expression vector pPho41 (Genentech), previously digested with the same restriction enzymes, and then transformed into *Escherichia coli* DH5a cells. Positive clones were sequenced (ABI) and transformed into protease-deficient *E. coli* expression strain 27C7 (ATCC 55244). Expression of PrP MHM2(106) was confirmed by growing cultures for 3 h at 37 °C in LB medium and 50 mg/mL ampicillin and then diluting them 100-fold into AP5 medium (Genentech) with 50 μg/mL ampicillin. Cells were grown at 37 °C and harvested 21 h later. The equivalent of $^{1}/_{10}$ OD_{600} unit of cell pellets was lysed in SDS loading buffer, loaded onto an 18% SDS−PAGE gel, and analyzed by Coomassie staining and Western blots. Large-scale expression and purification were carried out as described previously for other prion proteins (*25*). In short, *E. coli* paste was resuspended in 25 mM Tris-HCl (pH 8.0) with 5 mM EDTA (buffer A) and centrifuged. The pellet was resuspended in buffer A, passed through a microfluidizer (Microfluidics International, model MF110), and centrifuged for 1 h, after which the supernatant was discarded and the pellet subsequently solubilized in 8 M GdnHCl, 25 mM Tris-HCl, and 100 mM DTT (pH 8.0) and purified first by SEC and then by C4 reversed-phase HPLC. After each chromatographic step, fractions containing the rPrP106 were identified by SDS−PAGE with Western blotting. Purified rPrP106 was lyophilized and stored at −80 °C. The protein identity was confirmed by SDS−PAGE and mass spectrometry using a PE Biosystems Mariner orthogonal acceleration time-of-flight mass spectrometer equipped for electrospray ionization. The protein was seen to be a single pure species with a molecular mass of 11 570.13 Da, compared with a calculated value of 11 570.24 Da, assuming the presence of a single disulfide bond. The absence of free sulfhydryls was confirmed by mass spectrometry; the molecular mass of rPrP106 did not change after treatment with iodoacetic acid under conditions that would carboxymethylate free cysteine residues.

CD and Fluorescence. CD spectra were recorded with a Jasco J-720 CD spectrometer (Jasco, Easton, MD) scanning at 20 nm/min, with a bandwidth of 1 nm, and data spacing of 0.5 nm using 0.01, 0.1, 1, and 5 cm cuvettes. CD spectra were measured after incubation for 1 week at 23 °C, and did not change after an additional week of incubation. Background spectra were subtracted, and the data were converted to mean residue ellipticity, on the basis of known solute concentrations. Each spectrum that is shown represents the accumulation of three or more individual spectra. The secondary structure content was calculated by deconvolution of far-UV CD spectra as described in ref *26*.

Fluorescence spectra were monitored using a Perkin-Elmer LS50B (Perkin-Elmer, Waltham, MA) spectrofluorimeter (excitation at 278 nm, slit width of excitation and emission of 5 nm) in 0.4 cm rectangular cuvettes, and all data were corrected for the contribution of the respective solute concentrations.

Analytical Size-Exclusion Chromatography. For the experiments, we employed a TSK-3000 HPLC gel filtration column (300 mm × 7.80 mm). For the GdnHCl-induced denaturation experiment, rPrP106 samples were incubated with GdnHCl for 7 days prior to SEC analysis. The SEC column was equilibrated with the same concentration of GdnHCl [in 20 mM sodium acetate buffer (pH 5.4)]. All separations were performed at room temperature (23 °C) with a flow rate of 0.75 mL/min. To take into account anticipated changes in the permeation properties of the column that occur as a function of denaturant concentrations, we calculated partition coefficients (K_d) for each concentration of GdnHCl from the equation

$$K_d = (V_e - V_o)/(V_i - V_o)$$

where V_e is the elution volume of the protein sample, V_o is the void volume represented by the elution volume of blue dextran, and V_i is the full volume available for low-molecular mass compounds represented by the elution volume of aminobenzoic acid.

The column was calibrated using cytochrome *c* (Stokes radius of 1.73 nm), myoglobin (2.08 nm), carbonic anhydrase (2.4 nm), BSA (3.37 nm), and ferritin (6.79 nm) under native conditions, and cytochrome *c* (3.04 nm), myoglobin (3.78 nm), and carbonic anhydrase (5.13 nm) under denaturing conditions, using previously reported Stokes radii (*27*). To produce denatured proteins, samples of standard proteins were incubated at 23 °C for 4 h in 6 M GdnHCl and 10 mM DTT, and their elution volume was determined using the same denaturing conditions. The Stokes radius (Sr) of a protein is proportional to $1/K_d$ with a correlation coefficient of 0.99 as described by the equation

$$Sr = 0.022 + 1.36/K_d$$

The equation was used to estimate the dimensions of species formed by rPrP106. The square variance was measured as the square of the width determined at 60% of the peak height. This provides information about heterogeneity of the species eluted within a particular peak. Assuming no sorption effect, any increase of the square variance over the value determined for standard proteins indicates either that more than one ensemble of species is present in a particular peak or that interconversion occurs between different ensembles (*28*, *29*). In this case, the $1/K_d$ value represents a weighted average size of all species eluted with a particular peak.

Dynamic Light Scattering. All measurements were carried out using a DynaPro-801 TC Dynamic Light Scattering Instrument (Protein Solution Inc.). Samples (30 μL) were filtered through 100 nm membrane filters (Whatman Inc.), placed in DynaPro-MSTC's quartz cuvette, and measured at a constant temperature of 23 °C. After accumulation of at least 30 data points, experimental data were analyzed with both DYNAMICS version 4.0 and DynaLS software, which use three independent algorithms: cumulants (bimodal) analyses, the regularization fit, and the DynaLS non-negative least-squares (inverse Laplace transform) analyses.

Negative Staining and Electron Microscopy. Negative staining was performed on carbon-coated 600-mesh copper grids that were glow discharged prior to staining. Samples were adsorbed for 30 s, stained with freshly filtered 2% ammonium molybdate or 2% uranyl acetate, and after drying were viewed in a JEOL JEM 100CX II electron microscope at 80 kV at standard magnifications of 40000 and 80000. The diameter of the particles was measured on highly magnified prints of 80000× negatives. Measurements were made parallel to one side of the print, independent of the orientation of the particles. The magnification was calibrated using negatively stained catalase crystals.

Proteinase K Digestion. rPrP106 (≥1 mg/mL concentration) was incubated for at least 3 h at 23 °C under two different solution conditions: 1 M GdnHCl/20 mM sodium acetate buffer (pH 5.5) and 1 mM sodium acetate buffer (pH 5.5) without GdnHCl before addition of proteinase K. The proteinase K to protein ratio (1:50) was kept constant in each experiment. In the course of PK digestion performed at 23 °C, aliquots were withdrawn, the digestion was stopped by adding phenylmethanesulfonyl fluoride (PMSF) to a final concentration of 1 mM, and samples were analyzed by SEC, CD, fluorescence, mass spectrometry, and 16% Tricine SDS−PAGE with silver staining. In the presence of 1 M GdnHCl, proteinase K maintains 50% of its specific activity.

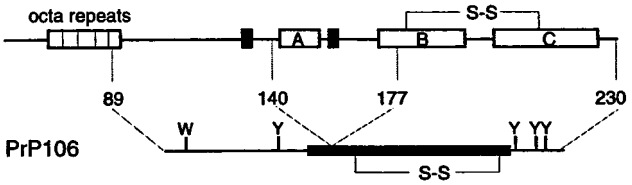

FIGURE 1: Schematic diagram of full-length PrP and PrP106. The octarepeats, three α-helices (A−C), and the two β-strands that are highlighted are shown for full-length PrP. PrP106 includes residues 89−140 and residues 177−230 of full-length PrP with the intact disulfide bond (mouse numbering). The single Trp and four Tyr residues of PrP106 are shown by vertical bars. The proteinase K-resistant β-sheet core of rPrP106 (residues 134−215) is defined by a bold line.

HPLC Mass Spectrometry. The proteinase K digestion products of rPrP106 were separated by reversed-phase HPLC and analyzed by MS. HPLC was carried out with an Applied Biosystems 140B syringe pump solvent delivery system (PE Biosystems, Foster City, CA), using a 1 mm × 150 mm C-18 Vydac column with a 300 Å pore size and a 5 mm particle size, connected to a 759A UV detector with a 35 nL capillary flow cell. Solvent A was 0.1% TFA and solvent B acetonitrile/0.08% TFA, with a linear gradient of 5 to 95% B over the course of 30 min at a flow rate of 50 mL/min. The eluent was split so that ~10% was introduced into the electrospray ionization source of the mass spectrometer mentioned above. Mass spectra were recorded continuously at 5 s intervals over the *m*/*z* range of 600−2000. UV chromatograms recorded at 215 nm were compared with total ion current (TIC) traces obtained from the mass spectrometer. ESIMS spectra corresponding to peaks in the UV and TIC traces were selected for averaging and deconvoluted using the software provided with the mass spectrometer, or spectra containing signals from multiple unresolved peptides were deconvoluted manually by visual inspection and selection of related multiply charged ions. Deconvolution converted each multiply charged ion series into a single peak of zero charge, giving the relative molecular masses of the peptides. The experimentally determined values were compared with calculations for all possible fragments of the rPrP106 MHM2 sequence. The calculated values were based on monoisotopic atomic masses for the smaller peptides (<3000 Da) and average masses for the larger peptides, for which the isotopic components could not be resolved.

RESULTS

Figure 1 shows the polypeptide PrP106 with two large deletions, Δ23−88 and Δ141−176. The N-terminal deletion (Δ23−88) removes the octarepeat regions that contain the Cu^{2+} binding sites (*4*, *19*−*21*). The deletion of residues 141−176 removes the first of the three helices of PrP^C while preserving the disulfide bond.

Concentration-Dependent Conformational Transition of rPrP106. Using CD, we have examined the rPrP106 conformation as a function of protein concentration using

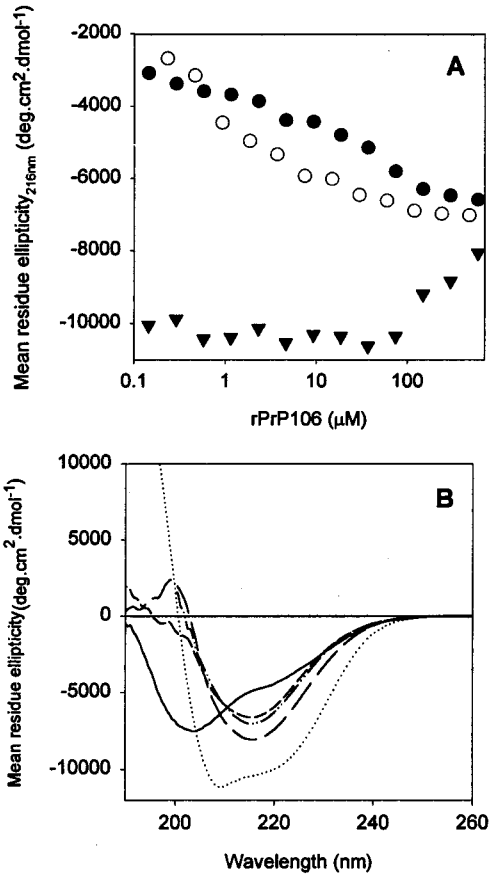

FIGURE 2: (A) Mean residue ellipticity of rPrP106 monitored as a function of protein concentration at 216 nm in dilute aqueous solution (●), in 0.2 M NaCl (○), and in 20% TFE (▼). (B) CD spectra of rPrP106 measured in the absence of salt (- - -), in 0.2 M NaCl (—••—), in 20% TFE (— — —) at a protein concentration of 0.6 mM, in dilute aqueous solution (—), and in 20% TFE (•••) at a protein concentration of 18 μM. All samples were prepared in 1 mM sodium acetate buffer (pH 5.5) and were incubated for 2 weeks at 23 °C in the corresponding solvent before CD measurements were taken.

three different solution conditions: (1) dilute aqueous solution, (2) 0.2 M NaCl, and (3) 20% TFE (Figure 2A). When rPrP106 was incubated in dilute aqueous solution [1 mM sodium acetate (pH 5.5)], far-UV CD spectra of samples with low protein concentrations (up to 30 mM) exhibited a minimum at 202 nm, an indication of a disordered conformation (Figure 2B). With increasing protein concentrations, we observed a conformational transition (in the range of 30−100 mM) characterized by the decrease in the ellipticity at 202 nm and the appearance of a new minimum at 216 nm (Figure 2B). If rPrP106 was incubated with 0.2 M NaCl, a similar structural transition was monitored at much lower protein concentrations (0.5−5 μM) (Figure 2A). CD spectra with a considerable α-helical contribution were observed for rPrP106 prepared in 20% TFE when the protein concentration was less than 100 μM. Nevertheless, increasing the rPrP106 concentration above 100 μM induced the conformational transition characterized by the appearance of the single minimum at 216 nm (Figure 2A,B). Dilution of the sample to the pretransition range of the concentrations did not induce any further change in the CD spectra over periods of at least 1 week. Thus, the concentration-dependent formation of this β-sheet-rich form was effectively irreversible.

Regardless of the solution conditions used (in low and high salt and in 20% TFE at pH 5.5), increasing the rPrP106 concentration facilitated the transition of rPrP106 to a state of high β-sheet content. In addition, the mean residue molar ellipticity monitored at 216 nm in three different solution conditions approached a similar level upon concentration-dependent conversion, suggesting that the post-transition states contain a similar amount of β-sheet structure, regardless of the solution conditions (Figure 2A). In contrast, the far-UV CD spectra monitored at lower protein concentrations are different from each other, illustrating that the pretransition state is intrinsically more flexible and adopts a solution-dependent secondary structure. As an example, the CD spectra of rPrP106 with a concentration corresponding to the pretransition region have significant contributions of random coil conformation with some signature of residual secondary structure in aqueous solution, whereas 20% TFE induces α-helix in the pretransition state with no signature of the random coil conformation. Most notably, the concentration-dependent transition is significantly facilitated by physiological salt concentrations. This occurs at a sub-micromolar concentration of rPrP106 in 0.2 M NaCl, whereas in the presence of TFE, a much higher concentration of protein (>100 μM) is required for conversion to the β-sheet-rich state.

The concentration-dependent conformational transitions of rPrP106 point to changes in the oligomerization state of PrP. Upon centrifugation of rPrP106 at 100000*g* for 1 h, the protein was found only in the supernatant. Because rPrP106 oligomers are soluble at a high concentration (0.6 mM) at room temperature, we studied the oligomerization states of rPrP106.

Analysis of the Oligomerization States. Using dynamic light scattering, we estimated the Stokes radii of the species, the formation of which is concentration-dependent (Figure 3). We found that rPrP106 assembles into particles with an average Stokes radius of 3.0 nm upon incubation in dilute aqueous solution, whereas in the presence of 0.2 M NaCl and in 20% TFE, the average Stokes radius of the particles was 5.5 nm. The Stokes radius obtained for each sample was largely independent of the algorithm used for calculation (Figure 3A). The fact that two distinct oligomeric states formed under different conditions is illustrated by the two separable populations (Figure 3B). The observation of relatively narrow distributions for each population argues that oligomerization is specific, although small amounts of larger aggregates with Stokes radii of 15−20 nm were detected in all samples (less than 0.6% based on the mass). No change in aggregation state was observed upon incubation of samples for a period of 2 weeks at room temperature. Assuming a spherical shape, the apparent molecular mass of 3.0 nm particles lies in the range of 50−70 kDa, whereas the molecular mass of the 5.5 nm species has to be between 150 and 300 kDa.

Negative stain electron microscopy shows a very homogeneous population of spherical particles for rPrP106 assembled in 1 mM sodium acetate at pH 5.5 (Figure 3C). The average diameter of 6.5 nm [standard deviation (SD) of 1.7 nm, $n = 125$] agrees well with the Stokes radius measured by dynamic light scattering. rPrP106 assembled in 20% TFE shows a somewhat larger particle size of 10 nm (SD of 3 nm, $n = 125$), also in excellent agreement with the light scattering data (Figure 3D). Histograms of the size distribu-

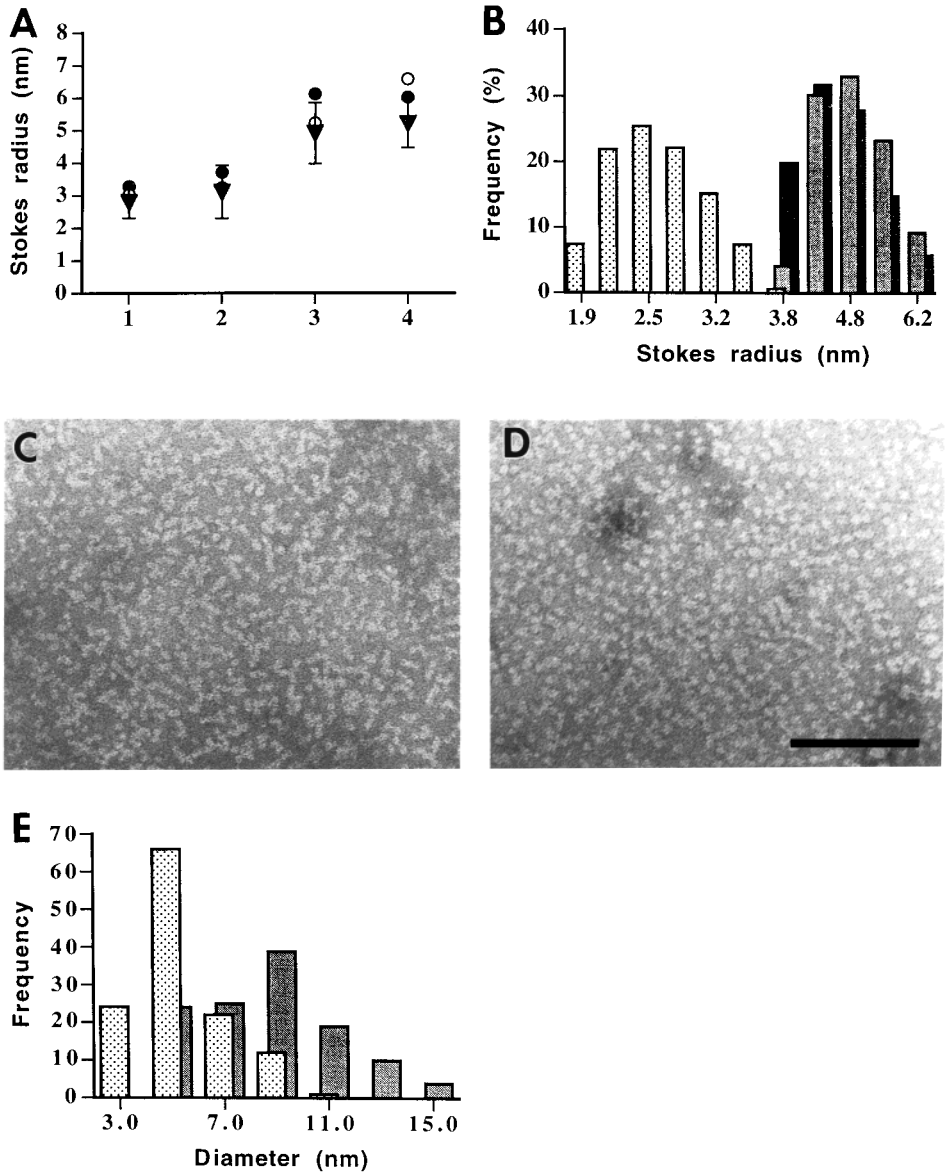

FIGURE 3: (A) Stokes radius of rPrP106 species estimated by dynamic light scattering after incubation of samples for 30 min (1) and 2 weeks (2) in dilute aqueous solution, for 2 weeks in the presence of 0.2 M NaCl (3), and for 2 weeks in the presence of 20% TFE (4). Stokes radii were calculated with three different algorithms: cumulative bimodal distribution (●), regularization fit (○), and DYNALS (▼). (B) Distribution of population vs Stokes radius calculated according to the DYNALS algorithm for rPrP106 incubated in dilute aqueous solution (stippled bars), in 0.2 M NaCl (black bars), and in 20% TFE (gray bars). (C and D) Electron micrographs of negatively stained rPrP106 assembled in dilute aqueous solution (C) and in 20% TFE (D). (E) Histograms of particle sizes estimated from electron micrographs of rPrP106 in dilute aqueous solution (stippled bars) and in 20% TFE (gray bars). All samples were prepared in 1 mM sodium acetate buffer (pH 5.5).

tions measured from electron micrographs provide independent evidence that two distinct populations of particles are formed under different solution conditions (Figure 3E).

Preliminary studies of the oligomerization process using the TSK-3000 size-exclusion column demonstrated that rPrP106 interacts with the column when SEC is performed in dilute aqueous buffer. Binding was completely abolished in the presence of ≥1 M GdnHCl. As shown in Figure 4, we observed two peaks when rPrP106 was prepared in 1 M GdnHCl. Upon incubation of the protein at room temperature, the area of the second peak was observed to decrease concomitantly with an increase in the area of the first peak. This process reached an apparent equilibrium after 1 week. We did not observe any change in the elution time of either peak during the course of the experiment. The combined area of absorption at 220 nm of the two peaks did not change either, suggesting that the species separated by SEC have a similar absorption coefficient at this wavelength. The CD spectra of the species eluted with the first peak exhibited a minimum at 217 nm, characteristic of β-sheet conformation, whereas the far-UV CD signal of the second peak gave no clear indication of either α-helical or β-sheet conformation (data not shown).

The observation of only two populations of species separated by SEC suggests cooperative self-assembly of rPrP106. Because the cooperativity of folding and/or assembly is a condition characteristic of a unique tertiary structure, we explored the cooperativity of self-assembly of rPrP106 by monitoring GdnHCl-induced equilibrium denaturation using both SEC and CD.

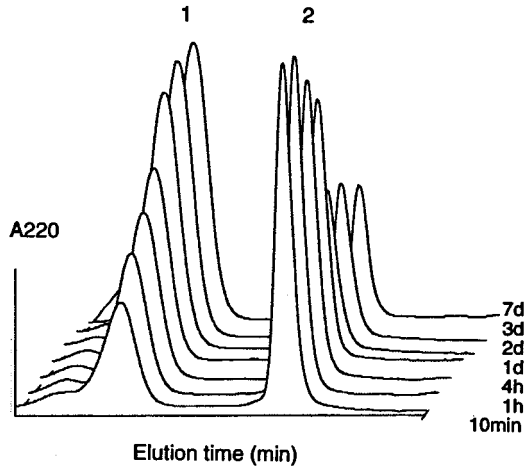

FIGURE 4: SEC profiles monitored during the time course of rPrP106 incubation in 1 M GdnHCl. Peaks 1 and 2 correspond to rPrP106 in different oligomer states. The rPrP106 fraction from C4 HPLC was lyophilized and dissolved in 1 M GdnHCl/20 mM sodium acetate buffer (pH 5.5) and incubated at 23 °C for 10 min, 1 h, 4 h, 1 day, 2 days, 3 days, and 7 days (from bottom to top). SEC was performed using a TSK-3000 column equilibrated with 1 M GdnHCl/20 mM sodium acetate buffer (pH 5.5) with a flow rate of 1 mL/min, and peaks were detected by absorption at 220 nm.

SEC can monitor three parameters as a function of GdnHCl: (1) Stokes radius, (2) heterogeneity of the species eluted within a particular peak, estimated on the basis of the square variance of each peak, and (3) the integrated UV absorbance of each peak, which is proportional to the population of each different oligomer state. Regardless of the GdnHCl concentration that was used, only two peaks were observed by SEC with no indication of intermediate species (data not shown). The Stokes radius of the species eluted with the second peak did not increase significantly with addition of GdnHCl, whereas the species eluted with the first peak expanded from 5.5 nm in 1 M GdnHCl to 9 nm in 6 M GdnHCl (Figure 5A). Because the linear working range of the SEC column was for particles with Stokes radii of 1.5−7 nm, the apparent increase in radius beyond 7 nm could be partly explained by a nonlinear dependence of the partition coefficient. However, it should be noted that the values of Stokes radii measured by SEC and light scattering in 2 M GdnHCl were in good agreement with each other (Figure 5A). The extrapolation of the Stokes radius measured in the presence of GdnHCl toward zero denaturant concentration gives an estimate of the dimension under nondenaturing conditions. By such an extrapolation, we found that the oligomeric species formed upon incubation in 0.2 M NaCl, in 20% TFE, and in GdnHCl all had similar Stokes radii. Under conditions that would reduce the disulfide bond, the Stokes radius increased only for the species eluting in the second peak. This Stokes radius is consistent with the dimensions of either the 10−13 kDa unfolded protein or the 50−70 kDa folded protein (*27*).

As shown in Figure 5B, the square variance of the second peak did not vary with GdnHCl concentration and corresponded to the square variance of the homogeneous species estimated as the square variance of standard proteins (Figure 5B). The square variance of the first peak was considerably higher than anticipated for a homogeneous species (Figure 5B). Such deviation can be due to the presence of species of different sizes (structural heterogeneity) or the rapid

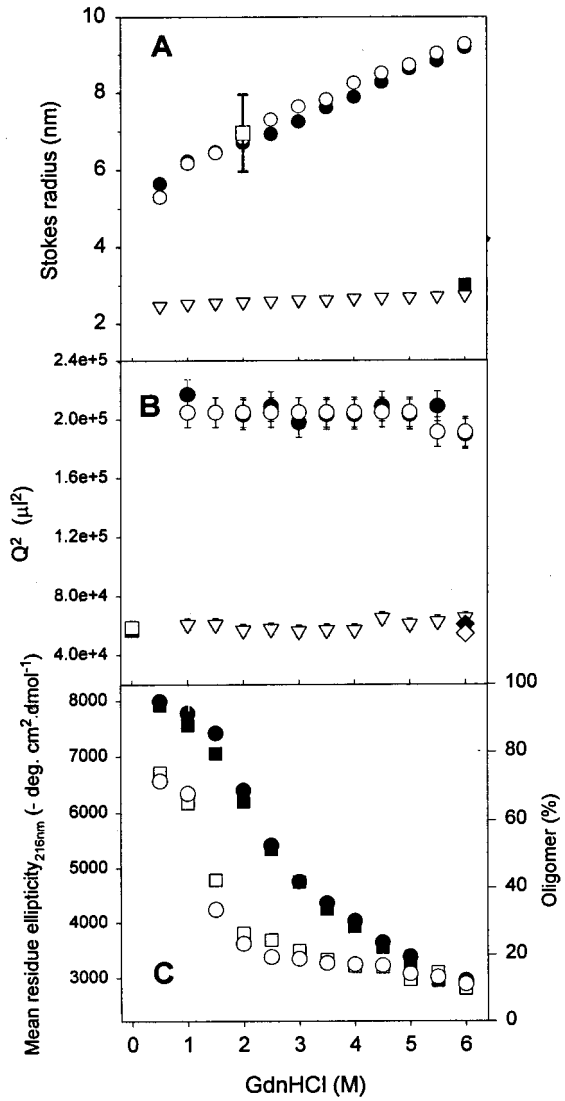

FIGURE 5: GdnHCl-induced equilibrium denaturation of rPrP106 monitored by SEC and CD at two different protein concentrations: 3.6 μM (white symbols) and 43 μM (black symbols). rPrP106 was incubated in different concentrations of GdnHCl with 20 mM sodium acetate buffer (pH 5.5) for 1 week at 23 °C before SEC and CD measurements were taken. (A) Dependence of the Stokes radius of the species eluted with peak 1 (circles) and with peak 2 (triangles) vs GdnHCl concentration. The Stokes radius determined under reducing conditions (in 10 mM DTT) is shown by ■. The Stokes radius estimated by light scattering using the DYNALS algorithm in 2 M GdnHCl is shown by □ with an error bar. (B) Dependence of the square of variance of the chromatographic peaks on GdnHCl concentration for the first peak (circles) and the second peak (triangle). The square variances for standard proteins in the native and denatured conditions are shown as reference values: for aprotonin (■) and carbonic anhydrase (□) in the absence of GdnHCl and for myoglobin (◆) and carbonic anhydrase (◇) in the presence of 6 M GdnHCl. (C) The mean residue ellipticity monitored at 216 nm (squares) and the oligomer population calculated from SEC (circles) are presented as a function of GdnHCl concentration.

interconversion between the oligomeric states of different sizes (dynamic heterogeneity). Taking into account the fact that the square variance of the first peak was not affected by addition of the denaturant or by changes in the total protein concentration in the range of 0.5−500 mM (data not shown), these facts do not support additional denaturant- or concentration-dependent interconversion between the oligomeric states of different sizes (dynamic heterogeneity) (Figure 5B). Dynamic heterogeneity also is inconsistent with

the irreversibility of the conversion. Hence, the first peak is composed of a structural ensemble of self-assembled oligomeric species with an average Stokes radius of 5.5 nm and a high content of β-sheet conformation.

Several lines of evidence suggest that the species eluted with the second peak was unfolded monomer rather than partially or fully folded oligomer. These include the absence of a clear signature for α-helical and β-sheet conformations; the absence of the denaturant-dependent conformational transition anticipated for folded multimer, as follows from gradual expansion of the dimension and from the behavior of the square variance (Figure 5A,B); and the absence of the concentration-dependent transition that was observed using SEC for the range of protein concentrations from 0.5 to 500 mM in the presence of 1 M GdnHCl (data not shown). Hence, our data indicate that only two states exist in the GdnHCl-induced equilibrium denaturation: the folded oligomer represented by the first peak and the unfolded monomer represented by the second peak.

Taking into account the fact that the absorption coefficient at 220 nm does not depend on oligomerization state, the area under the peaks provides an estimate of the respective populations of the oligomer and the monomer. Figure 5C presents the GdnHCl-induced transitions monitored as a change in the population of the oligomer together with mean residue ellipticity measured by CD at 216 nm. The conformational transitions measured by two observables were found to be cooperative, and they follow each other, reminiscent of a two-state transition for protein folding. The fact that two individual transitions are superimposable indicates that the oligomeric state maintains its structural integrity with equal amounts of secondary structure, independent of GdnHCl concentration. In contrast to the two-state model used to describe equilibrium protein folding and unfolding, the denaturant-induced transition of "monomer to oligomer" is concentration-dependent. Thus, at a protein concentration of 3.6 μM, the midpoint of the transition was 1.3 M GdnHCl, whereas the transition determined at 43 μM rPrP106 had a midpoint at 2.6 M GdnHCl. Hence, attempts to estimate the thermodynamic stability of the β-oligomer of PrP using a two-state model of equilibrium denaturation would not be appropriate without taking into account additional factors, such as protein concentration. Taking into account the common tendency of PrP molecules to oligomerize upon transition to the β-sheet isoform, we consider that denaturant- and temperature-induced unfolding experiments cannot estimate the true thermodynamic parameters for the β-isoform, as has been reported recently (*30*, *31*), unless evidence for a concentration-independent transition can be obtained.

SEC and CD data illustrate that the oligomeric state gradually expands in size as a function of denaturant concentration while maintaining its integrity and a constant level of β-sheet structure. Such a gradual expansion is usually considered to be a property of the unfolded state rather than of the folded state (*28*). In the case of the folded oligomer, the gradual increases of the radius can be explained by the expansion of the solvent-exposed, partially unfolded N-terminal region of assembled polypeptide chains with addition of denaturant, as will be illustrated below. Hence, the GdnHCl-induced equilibrium unfolding experiment demonstrates that the process of rPrP106 oligomerization is a two-state cooperative self-assembly of monomeric to oligomeric

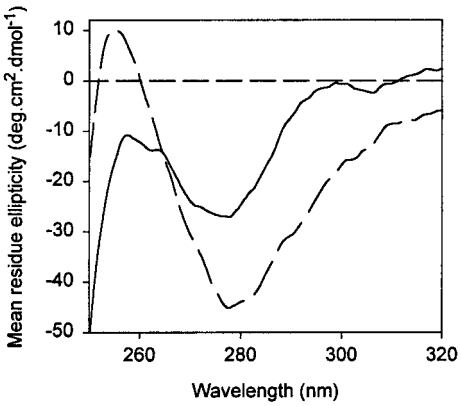

FIGURE 6: Near-UV CD spectra of a 0.3 mM rPrP106 solution measured after incubation for 2 weeks in 1 mM sodium acetate buffer (pH 5.5) at 23 °C (− − −) and measured 5 min after dissolution of rPrP106 in 8 M GdnHCl/20 mM NaCl (pH 5.5) (—). The spectra are the averages of six scans that have been corrected by subtracting corresponding blanks.

species accompanied by the conformational transition to the β-sheet conformation. It should be noted that in our experiments we are not able to separate any kinetic intermediate in the rPrP106 self-assembly process, suggesting that the process of oligomer formation is faster than the time scale of SEC (15 min). The fact that about 12% of the rPrP106 population remains oligomeric after incubation for 1 week with 6 M GdnHCl illustrates the unusually high stability of the β-sheet conformation.

Deconvolution of far-UV CD spectra demonstrated that about 40% of the amino acid residues are involved in the β-sheet structure upon self-assembly of rPrP106, whereas only 5−10% are α-helical. Because the ability to induce neuropathologic changes in vivo is associated with PrP isoforms enriched in β-structure, we attempted to identify the region of rPrP106 that is responsible for formation of the β-sheet structure.

Insight into the Structural Organization of Self-Assembled Species. The cooperativity observed in the GdnHCl-induced denaturation indicates that a unique tertiary structure is formed upon self-assembly of the polypeptide chains. As shown in Figure 6, assembled rPrP106 exhibits a near-UV CD signal that does not disappear, even in the presence of 8 M GdnHCl. This suggests that at a high protein concentration (0.3 mM) the assembled state is still populated even under strongly denaturing conditions.

Because rPrP106 contains five intrinsic fluorescence probes (one Trp residue located in the N-terminus and four Tyr residues, three of which are at the C-terminus of the polypeptide; see Figure 1), we were able to employ fluorescence spectroscopy to monitor the aggregation state of rPrP106. Spectra were recorded for the assembled state (in 0.2 M NaCl at a protein concentration of 7 μM), a predominantly monomeric state (in 1 mM sodium acetate at 1 mM protein), and under highly denaturing conditions (6 M GdnHCl at 1 μM protein). Figure 7B shows the fluorescence emission spectra monitored upon excitation at 278 nm, in which signals arise from tyrosine and tryptophan residues. These spectra can also indicate energy transfer from Tyr to Trp. Similar spectra with maxima at 304 and 350 nm were observed for all three samples regardless of the oligomer state. Separate maxima for Tyr at 304 nm and for Trp at

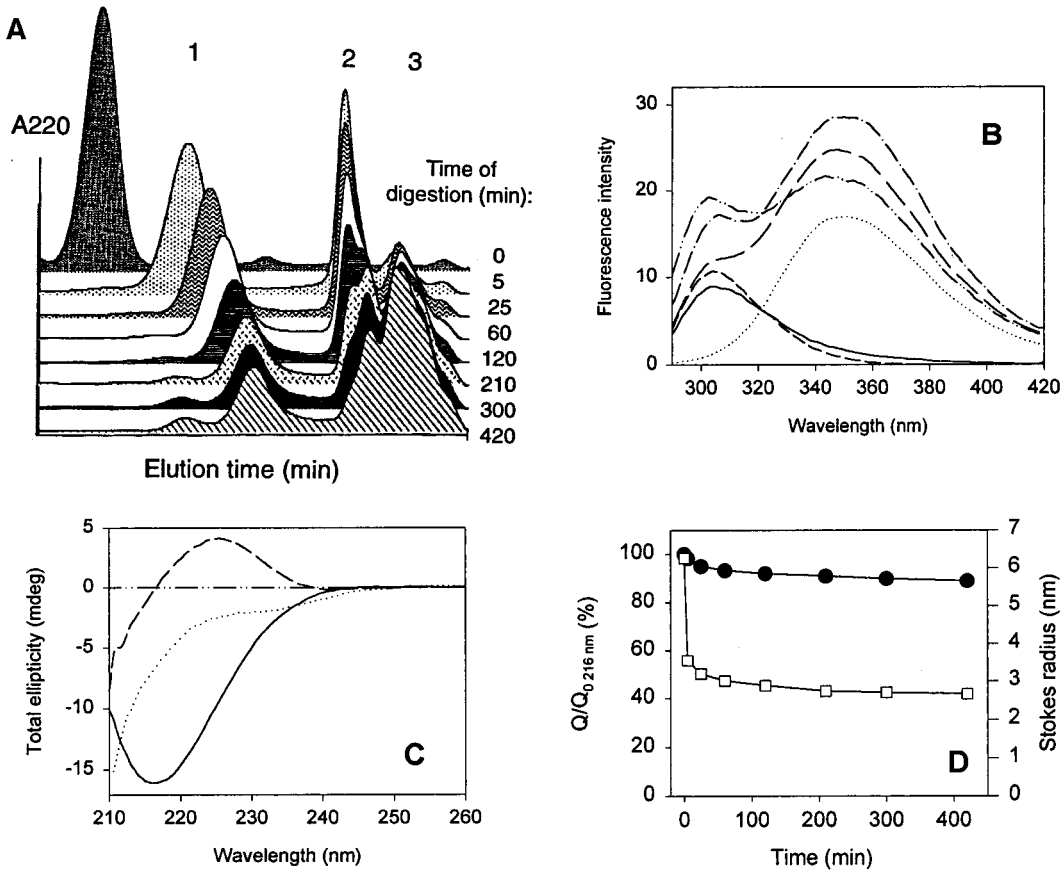

FIGURE 7: Analysis of the products of proteinase K digestion (1:50 proteinase K:protein ratio) of rPrP106 self-assembled in 1 M GdnHCl/20 mM sodium acetate buffer (pH 5.5). (A) The time course of proteinase K digestion monitored by SEC in 1 M GdnHCl with a flow rate of 0.75 mL/min and detected by absorption at 220 nm: before addition of proteinase K and upon incubation for 5, 25, 60, 120, 210, 300, and 420 min with proteinase K. (B) Fluorescence emission spectra of the products separated by SEC after PK digestion for 5 min: peak 1 (—), peak 2 (•••), and peak 3 (- - -). The fluorescence spectra of full-length rPrP106 are shown for reference: in 1 mM sodium acetate buffer (—••—) and in 6 M GdnHCl (—•—) with a protein concentration of 1 μM and in 0.2 M NaCl (— — —) with a protein concentration of 7 μM (the fluorescence intensity for the last sample was recalculated on a millimolar basis). (C) Far-UV CD spectra of the products separated by SEC after proteinase K digestion for 300 min: peak 1 (—), peak 2 (•••), and peak 3 (- - -). CD and fluorecsence spectra were measured 5 min after collection of SEC fractions. (D) Kinetics of proteinase K digestion monitored as a percentage of the ellipticity signal at 216 nm calculated relative to the ellipticity signal at time zero ($100Q/Q_0$) (●) and by the Stokes radii of species eluted with the first peak (□). All CD and fluorescence spectra have been corrected by subtracting corresponding buffer blanks and taking into account the amount of proteinase K in some CD samples.

350 nm, as well as similar quantum yields observed for all three spectra, do not support efficient transfer of energy from Tyr residues to the single Trp in the assembled state, indicating that the N- and C-termini are not adjacent to each other when rPrP106 is assembled. We judge the Trp to be in a polar environment given that the fluorescence maximum is at 350 nm for all samples. Hence, the fluorescence data suggest that the N-terminus and probably the C-terminus are exposed to the solvent in the assembled state.

To localize the regions of rPrP106 that adopt stable ordered conformations in an oligomeric state, we performed limited proteinase K digestion in 1 M GdnHCl and analyzed the products of cleavage using SEC, far-UV CD, fluorescence, and SDS−PAGE. As has been shown before in 1 M GdnHCl, rPrP106 assembles into the oligomeric species with an average Stokes radius of 6 nm. As shown in Figure 7A, about 98% of the polypeptide is in the oligomeric state at time zero of proteinase K digestion. The oligomer with a 6 nm Stokes radius disappeared completely after incubation for just 5 min with proteinase K; instead, three new populations of products were separated by SEC (peaks 1−3). The species eluted in the first peak exhibited weak fluorescence with maxima at 304 nm (typical for Tyr), profound β-sheet conformation, and a Stokes radius of 4.3 nm after digestion for 5 min, which decreased gradually upon additional incubation with proteinase K, reaching the steady-state level of 2.7 nm (Figures 7B,C and 8D). The species corresponding to the second peak had fluorescence maxima of 350 nm, characteristic of Trp; the CD spectra show a high content of the random coil conformation and a slight signature of the residual structure. The species of the third peak had fluorescence spectra typical for Tyr residues and CD spectra similar to a left-handed poly-L-proline type II helix. The SEC profiles demonstrated continuous change in the shape and the elution time of the second and the third peaks, whereas the elution time of the first peak became stable after digestion for 4 h (Figure 7A). The very high resistance of the species in the first peak to proteinase K digestion and their profound β-sheet conformation are consistent with our suggestion that this represents a stable ordered core of the assembled species.

The SDS−PAGE gel depicted in Figure 8A shows that the final proteinase K-resistant products of cleavage of self-assembled rPrP106 have a molecular mass of 5−6 kDa.

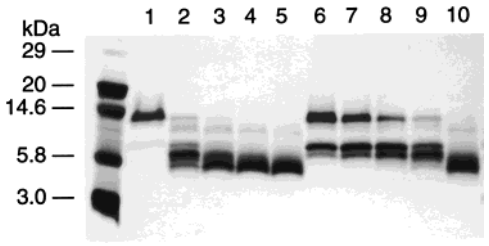

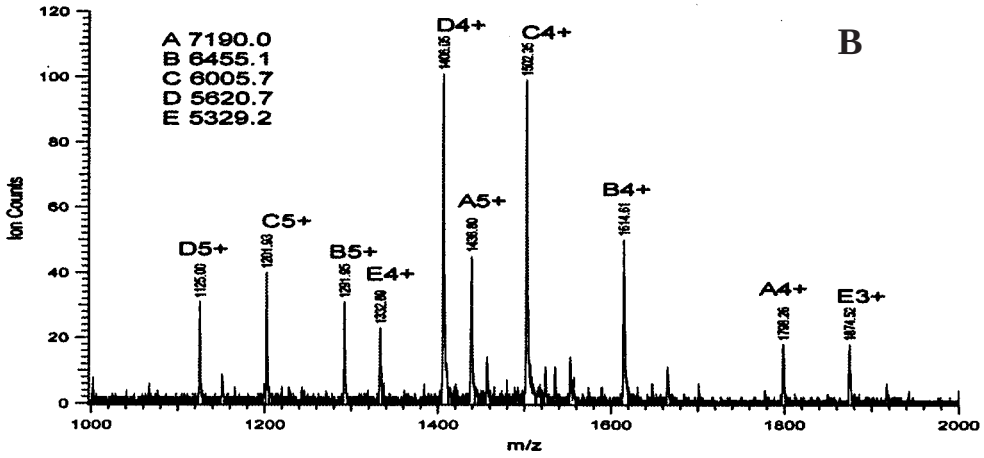

C

Proteinase K-resistant core after	Theoretical MW (Da)	Measured in 1M GndHCl	Measured in 1mM Na-acetate
6 min digestion			
116----------230	**8754.1**	**8754.3**	
134----------230	**7190.2**	**7190.0**	
134----------224	6455.4	6455.1	
134----------220	6006.0	6005.7	
1 h digestion			
134----------220	**6006.0**	**6005.7**	
134----------217	**5620.5**	**5620.7**	
134----------224	6455.4	6455.1	
134----------230	7190.2	7190.0	
134----------215	5329.2	5329.2	
6 h digestion			
134----------217	**5620.5**	**5620.7**	**5620.7**
134----------220	**6006.0**	**6005.7**	**6005.7**
134----------215	**5329.2**	**5329.2**	5329.2
134----------224	6455.4	6455.1	
134----------230	7190.2	7190.0	7190.0

FIGURE 8: Analysis of the products of rPrP106 cleavage during the course of proteinase K digestion. (A) SDS−PAGE of the products of digestion of rPrP106 self-assembled in 1 M GdnHCl/20 mM sodium acetate (2−5) and in 1 mM sodium acetate (6−10) at pH 5.5. rPrP106 before digestion (1) and after incubation for 5 min (2 and 6), 15 min (3 and 7), 30 min (4 and 8), 1 h (5 and 9), and 3 h (10) with proteinase K. The proteinase K:protein ratio was 1:50, and samples were incubated at 22 °C. (B) A spectrum from HPLC-MS analysis of PrP106 after digestion for 1 h, showing later eluting fractions not separated by HPLC. Manual analysis identified five peptides as shown in the inset table. Peptides C and D with the strongest signals are likely the most abundant species. Measured masses in the table are mean values from several analyses. (C) Proteinase K-resistant products of digestion of β-rPrP106 are identified using MS. Major products of digestion estimated according to the peak intensity of mass spectra are highlighted.

These products of proteinase K cleavage remained resistant to further digestion even when a higher proteinase K to rPrP106 ratio of 1:10 was used. In contrast, the monomeric form of the polypeptide was hydrolyzed completely after incubation for 20 min with proteinase K at a 1:50 ratio (data not shown). It is very surprising that a substantial reduction of the Stokes radius of the oligomeric state from 6.0 to 2.7 nm in the time course of proteinase K digestion is accompanied by a loss of only 10% of the intensity of the CD signal measured at 216 nm. This indicates that the core of assembled species remains intact, maintaining high β-sheet content (Figure 7D).

Having previously shown that rPrP106 self-assembles into oligomers characterized by two different Stokes radii of 3.0 and 5.5 nm under different solute conditions, we sought to test whether the propensity to form a β-conformation was solvent-dependent. Therefore, we analyzed the products of proteinase K digestion of both oligomeric forms. As shown in Figure 8A, the time-dependent patterns of proteolytic fragmentation for rPrP106 oligomers self-assembled in 1 M GdnHCl and in dilute aqueous solution seem to be different (compare lanes 2−4 with lanes 7−9). Although this indicates there are some differences in the structural organization of the two oligomers, the final products of proteinase K digestion have identical electrophoretic mobilities (compare lane 5 with lane 9).

Using mass spectrometry, we identified the core region of rPrP106 that is resistant to proteinase K digestion (Figure

Table 1: Biochemical Properties of Recombinant and Scrapie Isoforms of PrP

	multimeric state	solubility	proteinase K resistance	% α-helix/% β-sheet	N-sugars/GPI	infectivity
α-rPrP106 in 30% TFE	monomer	soluble	very sensitive	48/7 by CD	−/−	?
α-rPrP(90−231)	monomer	soluble	very sensitive	43/4 by NMR[a] 42/3 by FTIR[b]	−/−	−
β-rPrP106	oligomers with 3 and 5.5 nm Stokes radii	soluble up to 10 mg/mL	resistant core contains residues 134−215	5−10/40 by CD	−/−	?
β-rPrP(90−231)	oligomers (6−7mers)	soluble at low (<0.5 mg/mL) concentrations	sensitive	15/33 by CD	−/−	−
PrP^{Sc}106	prion rods	nonsoluble	resistant	27−31/36 by FTIR[c]	+/+	+
PrP 27−30	prion rods	nonsoluble	protease-resistant core of full-length PrP^{Sc}	21/54 by FTIR[b]	+/+	+

[a] Liu et al. (*7*). [b] Pan et al. (*43*). [c] Supattapone et al. (*1*).

8B,C). Analysis of the reaction mixture after digestion for 6 min revealed two major sites of cleavage located in the N-terminus (residues 116 and 134) and two sites in the C-terminus (residues 224 and 220). Upon incubation with proteinase K, a few new cleavage sites were found near the C-terminus, whereas the N-terminus was very resistant to proteolysis. Finally, three major proteinase K-resistant products of digestion of the oligomeric species assembled in 1 M GdnHCl were identified after incubation for 6 h with the enzyme (peptides 134−215, 134−217, and 134−222). Identical products of proteinase K digestion were found for the oligomeric species with a Stokes radius of 3.0 nm (Figure 8C). Thus, under a variety of conditions, rPrP106 assembles into an oligomeric state, where residues 134−215 retain proteinase K resistance. To maintain 90% of the initial mean residue ellipticity measured at 216 nm upon cleavage of more than 50% of the amino acid residues, about 80% of the residues of the 134−215 peptide should adopt a β-sheet conformation. Because the β-sheet-rich core remains assembled in the oligomeric form, it is likely that β-structure is stabilized by intermolecular interactions.

DISCUSSION

The central event in the pathogenesis of prion diseases is a conformational transition of PrP from the α-helical PrP^{C} isoform to the predominantly β-sheet PrP^{Sc} isoform. Experimental evidence suggests PrP^{C} is a kinetically trapped state, and we have operationally defined PrP* as a transition state intermediate between PrP^{C} and PrP^{Sc}:

$$PrP^{C} \rightarrow PrP^{*} \rightarrow PrP^{Sc}$$

In this formalism, PrP* is a high-energy conformational isoform that is likely to be partially unfolded. Although NMR studies have provided structural details about the C-terminal α-helical domain of recombinant PrP (*5*−*8*), which appears to resemble PrP^{C}, the absence of similar information for PrP^{Sc} and intermediate states creates difficulties in understanding the molecular mechanism of prion replication.

Our recent studies have demonstrated that 50% of the PrP residues may be removed while the remaining polypeptide, PrP106, is able to form prions (*1*). The ability to support prion replication for such short polypeptides presents a new tool for studies of the mechanism of the conformational conversion. This result established that PrP106 retains regions that are necessary for prion formation, including the most conserved region of PrP (residues 110−130) (*32*) and the regions that form helices B and C in PrP^{C}, including the disulfide bridge (*5*−*8*) (Figure 1). Unlike full-length recombinant PrP^{C}, rPrP106 is largely unfolded in the monomeric state, but helical structure can be stabilized with the addition of TFE. Thus, it is possible that monomeric PrP106 represents a destabilized analogue of PrP^{C} on the path to PrP*.

Whether recombinant PrP106 folded to the β-rich conformation is a relevant model for PrP^{Sc}106 remains to be established. As shown in Table 1, PrP^{Sc}106 isolated from scrapie-infected mouse brains exhibits major features typical of PrP 27−30 such as resistance to limited proteolysis, dominance of β-sheet content over α-helical content, and insolubility in nondenaturing detergents upon purification (*1*). Here, we report that β-rPrP106 possesses some properties that are similar to those of PrP^{Sc}. After rPrP106 assembles into oligomers with a β-sheet content similar to that of PrP^{Sc}106 (Table 1), it becomes more resistant to limited proteinase K digestion than the monomeric rPrP106. The fact that rPrP106 assembles into β-oligomers under a variety of conditions illustrates a solvent-independent propensity to adopt a β-sheet-rich conformation upon association, suggesting that this conformation is the thermodynamically most stable multimeric form. While β-rPrP106 exhibits some features of PrP^{Sc}106, it also has several distinct properties. Thus, upon prolonged proteinase K digestion, β-rPrP106 retains a resistant core composed of amino acid residues 134−215, whereas PrP^{Sc}106 remains entirely resistant. It is likely that β-rPrP106 has a reduced amount of α-helical content as studied by CD relative to the PrP^{Sc}106 as measured by FTIR. The question of whether β-rPrP106 can be infectious is currently under investigation. In contrast to PrP^{Sc}106, β-rPrP106 forms soluble oligomers. Since the disulfide bond remains intact in both PrP^{Sc}106 and β-rPrP106, some differences in the biochemical properties such as solubility might be due to the absence of the GPI moiety as well as two N-linked sugars in rPrP106. Even though β-rPrP106 and PrP^{Sc}106 possess some distinctions, rPrP106 might represent a useful tool for studying the principles involved in the conformational transition to the β-rich state.

Implications for Models of PrP^{Sc} Formation. Two competing models have been proposed to explain replication of prions: template-assisted and nucleation-dependent polymerization (*3*, *33*). The template-assisted model postulates that rearrangement from α-helix to β-sheet constitutes a conformational distinction between PrP^{C} and PrP^{Sc} that creates a high kinetic barrier (Figure 9A) (*3*, *34*). Because conformational conversion has to proceed through a partially unfolded intermediate state (PrP*) that is highly unfavorable, the

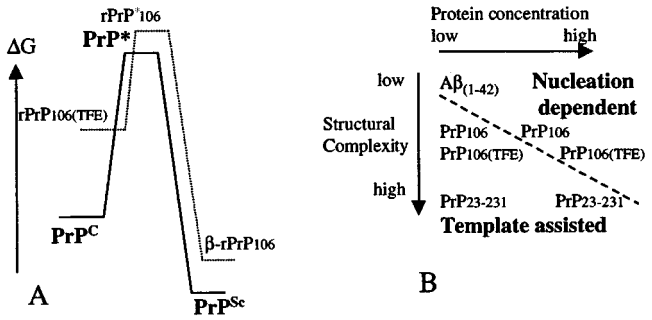

FIGURE 9: (A) Free energy diagram for the conformational transition of the monomeric α-isoform of prion protein (PrP^C) to the oligomeric β-isoform (PrP^{Sc}). The kinetic barrier between PrP^C and PrP^{Sc} is extremely high and cannot be crossed in a biologically relevant time. The barrier height is reduced substantially for PrP106 when the polypeptide is in an unfolded state (rPrP*106), while TFE delays the conformational transition by increasing the structural complexity of rPrP106 (α-rPrP106TFE). (B) The schematic diagram shows that the conformational conversion of Aβ, PrP106, and PrP23−231 can be described either by a template-assisted or by a nucleation-dependent model depending upon the structural complexity and the concentration of proteins.

template-assisted model assumes (1) that the transition from PrP^C to monomeric PrP^{Sc} is the rate-limiting step and thus (2) that the reaction is a first-order process. Mutations linked with familial prion diseases as well as exogenous inoculation of homologous PrP^{Sc} templates facilitate the conformational transition of PrP^C to PrP^{Sc} by decreasing the kinetic barrier between PrP^C and PrP^{Sc} isoforms (*34*). According to the nucleation-dependent mechanism, PrP^C exists in a fast equilibrium with monomeric PrP^{Sc} with little kinetic barrier separating PrP^C from PrP^{Sc}. In this model, the slowest step of PrP^{Sc} propagation is formation of the nucleus (the assembly of monomeric PrP^{Sc} into a small aggregated oligomeric form) that is followed by fast polymerization to the higher oligomerization state (*33*, *35*). Consequently, the nucleation step has to proceed as a higher-order reaction. Thus, each mechanism postulates a distinct rate-limiting step for PrP^{Sc} propagation that can be distinguished on the basis of the reaction order of PrP^{Sc} propagation. The template-assisted model relates the kinetic barrier with the structural complexity of the pretransition state (PrP^C isoform), whereas the nucleation-dependent model postulates that the low thermodynamic stability of the prenucleus (the oligomeric intermediate state during PrP^{Sc} formation) determines the slow rate of conformational conversion. Previous studies demonstrated that the length of scrapie incubation time is inversely proportional to the level of PrP^C expression in the brain, consistent with a first-order process in accord with the template-assisted model (*36*, *37*).

The data presented here illustrate that the deletion of 36 amino acid residues (Δ141−176), which include helix A and the loop between helices A and B (Figure 1), strongly destabilizes the α-helical isoform of PrP, which is a pretransition state. Thus, monomeric rPrP106 exhibits the characteristics that the template-assisted model predicts for the PrP* intermediate state, such as the absence of extensive secondary and tertiary structure, sensitivity to proteinase K digestion, and high solubility. Because monomeric rPrP106 is mostly unstructured, the template-assisted model assumes that the kinetic barrier for conversion to the β-oligomer is considerably reduced (Figure 9A). Our data demonstrate that rPrP106 assembles spontaneously to the thermodynamically stable oligomeric β-sheet isoform under the same conditions that recombinant Syrian hamster PrP folds to an α-helical isoform (*18*). At the same time, in the presence of 20% TFE, rPrP106 remains in an α-helical form upon incubation for 2 weeks even at protein concentrations as high as 100 μM, whereas unstructured rPrP106 at the same concentration undergoes complete conversion to the β-oligomer within 1 h (Figure 2). Only at protein concentrations higher than 100 μM does α-rPrP106 undergo conversion to the β-oligomer in TFE. Thus, the TFE-managed increase in the structural complexity of the pretransition state corresponding to the α-helix formation prevents transition to the β-oligomer, as expected by the template-assisted model (Figure 9A,B) (*34*). Since the template-assisted model suggests a connection between the structural complexity of the monomeric state and the height of the kinetic barrier, the induction and/or stabilization of any additional contacts in the pretransition state causes an increase in the kinetic barrier as shown in Figure 9A. It is more difficult to explain the effect of TFE on the conformational transition using a nucleation-dependent model because this model postulates fast equilibrium between pre- and post-transition states of the conformational conversion regardless of the structural complexity of both states.

The nucleation-dependent mechanism was developed to describe oligomerization of amyloid peptides Aβ(1−40) and Aβ(1−42) to the cross-β-sheet amyloid fibrils, the major component of Alzheimer's amyloid plaque (*33*, *35*). Because a similar conformational change accompanies propagation of PrP^{Sc}, the nucleation-dependent mechanism was applied to describe the conformational transition of PrP (*33*, *35*, *38*). In contrast to the monomeric Aβ peptides, which are unstructured (*39*), PrP^C exists in a stable conformation characterized by a unique secondary and tertiary structure with a tightly packed hydrophobic interior (*7*). Such a difference in the structural complexity between Aβ peptides and PrP^C is believed to be responsible for a fundamentally different oligomerization mechanism, resulting in a clear distinction in the rate-limiting step of the conformational transition (Figure 9B). Aβ and PrP^C can be considered two ends of a structural complexity spectrum, and their conformational conversion occurs according to the nucleation-dependent and template-assisted mechanisms, respectively. Monomeric rPrP106 occupies an intermediate position between Aβ and PrP^C in terms of structural complexity. Consequently, the conformational transition of rPrP106 to β-oligomer may correspond to either the template-assisted or the nucleation-dependent model, depending upon solvent conditions and protein concentration. As shown in Figure 9B, conformational conversion of rPrP106 resembles the nucleation-dependent mechanism when the pretransition state of rPrP106 is unstructured and the concentration of polypeptide is high enough, whereas the conformational transition occurs according to the template-assisted model at a lower concentration or when the pretransition state of rPrP106 is structured.

Recently, Chiti et al. and Guijarro et al. observed formation of typical amyloid fibrils for acylphosphatase and the SH3 domain of phosphatidylinositol 3-kinase, proteins that are not associated with any of the known amyloid diseases (*40*, *41*). Conformational conversion occurred under specific partially denatured conditions when the native states of the proteins were destabilized. The authors suggested that the

formation of ordered amyloid fibrils is a property that can be common for all natural polypeptide chains because the cross-β-sheet structure is stabilized by backbone hydrogen bonds, a principle that is focused on the general intrinsic property of polypeptide backbone, rather than on the specific side chain, sequence-dependent interactions. If the cross-β-sheet conformation is the most thermodynamically stable multimeric form for many proteins, it must be separated from the native state by a high kinetic barrier that most proteins never cross to remain in the native folded state. Only under certain partially denatured conditions can the kinetic barrier be reduced due to that loss of structural complexity. These studies support our observation of the relationship between structural complexity of the pretransition state and the ability to undergo conformational conversion. Hence, two experimental observations, the unusually short incubation time for PrP106-supported disease and the cooperative self-assembly of rPrP106 to a β-oligomer, support the idea that the kinetic barrier for the conformational conversion of this molecule is substantially reduced due to the low structural complexity of PrP106.

Insight into the Structural Organization of β-rPrP106. Several lines of evidence indicate that the oligomer of rPrP106 is stabilized by a β-sheet core within the region of residues 134−215. Upon cleavage of the N-terminal region, rPrP106 remains assembled in a β-sheet-rich conformation and maintains resistance to proteinase K digestion (Figures 7 and 8). Even though the β-rPrP106 gradually expands in size with the addition of denaturant, it preserves a stable β-sheet core that maintains the same amount of secondary structure and keeps the disulfide bond intact under highly denaturing reducing conditions (6 M GdnHCl/10 mM DTT) (Figure 5). Moreover, we found that the region of residues 134−215 of rPrP106 has a solvent-independent propensity to adopt a stable β-sheet conformation. The same region of residues 134−215 has been found to be protected from proteinase K digestion in both oligomeric forms with Stokes radii of 3.0 and 5.5 nm (Figure 8C).

Several lines of experimental study support the conclusion that the infectious properties of prions are enciphered in the tertiary and quaternary structure of PrP^{Sc} (*42*−*46*). Our data show that β-rPrP106 adopts a unique tertiary structure upon assembly as evidenced by near-UV CD spectra, a distinct pattern of proteinase K digestion products, and cooperative GdnHCl-induced unfolding. The GdnHCl-induced transition monitored by SEC and CD strongly indicates the presence of only two populated states in equilibrium denaturation, the folded β-oligomer and the unfolded monomer, which is reminiscent of a cooperative two-state process. With increasing denaturant concentrations, the oligomeric species undergo continuous expansion as measured by the Stokes radius, which is believed to be due to local unfolding without disruption of β-rich oligomer particles. The lack of detection of populated equilibrium intermediate states and the lack of an effect of the denaturant on the heterogeneity of the oligomeric ensemble demonstrate that β-rPrP106 is thermodynamically stable only when a certain critical number of monomers interact with each other. We have not found any evidence for a β-monomer of rPrP106 under equilibrium conditions. This implies that the β-sheet structure of the assembled rPrP106 is stabilized by intermolecular interactions. Our data do not allow us to make any conclusion about the actual kinetic pathway of the conformational transition. Thus, we cannot distinguish between monomer refolding to a β-rich structure prior to multimer assembly and multimer facilitating a conformational change in the monomer.

ACKNOWLEDGMENT

Mass Spectrometry was carried out in the University of California, San Francisco, Mass Spectrometry Facility.

REFERENCES

1. Supattapone, S., Bosque, P., Muramoto, T., Wille, H., Aagaard, C., Peretz, D., Nguyen, H.-O. B., Heinrich, C., Torchia, M., Safar, J., Cohen, F. E., DeArmond, S. J., Prusiner, S. B., and Scott, M. (1999) *Cell 96*, 869−878.
2. Prusiner, S. B. (1997) *Science 278*, 245−251.
3. Cohen, F. E., Pan, K.-M., Huang, Z., Baldwin, M., Fletterick, R. J., and Prusiner, S. B. (1994) *Science 264*, 530−531.
4. Viles, J. H., Cohen, F. E., Prusiner, S. B., Goodin, D. B., Wright, P. E., and Dyson, H. J. (1999) *Proc. Natl. Acad. Sci. U.S.A. 96*, 2042−2047.
5. Donne, D. G., Viles, J. H., Groth, D., Mehlhorn, I., James, T. L., Cohen, F. E., Prusiner, S. B., Wright, P. E., and Dyson, H. J. (1997) *Proc. Natl. Acad. Sci. U.S.A. 94*, 13452−13457.
6. James, T. L., Liu, H., Ulyanov, N. B., Farr-Jones, S., Zhang, H., Donne, D. G., Kaneko, K., Groth, D., Mehlhorn, I., Prusiner, S. B., and Cohen, F. E. (1997) *Proc. Natl. Acad. Sci. U.S.A. 94*, 10086−10091.
7. Liu, H., Farr-Jones, S., Ulyanov, N. B., Llinas, M., Marqusee, S., Groth, D., Cohen, F. E., Prusiner, S. B., and James, T. L. (1999) *Biochemistry 38*, 5362−5377.
8. Riek, R., Hornemann, S., Wider, G., Billeter, M., Glockshuber, R., and Wüthrich, K. (1996) *Nature 382*, 180−182.
9. Gabizon, R., McKinley, M. P., Groth, D., and Prusiner, S. B. (1988) *Proc. Natl. Acad. Sci. U.S.A. 85*, 6617−6621.
10. Bolton, D. C., McKinley, M. P., and Prusiner, S. B. (1982) *Science 218*, 1309−1311.
11. Prusiner, S. B., Bolton, D. C., Groth, D. F., Bowman, K. A., Cochran, S. P., and McKinley, M. P. (1982) *Biochemistry 21*, 6942−6950.
12. Prusiner, S. B., McKinley, M. P., Bowman, K. A., Bolton, D. C., Bendheim, P. E., Groth, D. F., and Glenner, G. G. (1983) *Cell 35*, 349−358.
13. Huang, Z., Prusiner, S. B., and Cohen, F. E. (1996) in *Prions Prions Prions* (Prusiner, S. B., Ed.) pp 49−67, Springer-Verlag, Berlin.
14. Heller, J., Kolbert, A. C., Larsen, R., Ernst, M., Bekker, T., Baldwin, M., Prusiner, S. B., Pines, A., and Wemmer, D. E. (1996) *Protein Sci. 5*, 1655−1661.
15. Nguyen, J. T., Inouye, H., Baldwin, M. A., Fletterick, R. J., Cohen, F. E., Prusiner, S. B., and Kirschner, D. A. (1995) *J. Mol. Biol. 252*, 412−422.
16. Zhang, H., Kaneko, K., Nguyen, J. T., Livshits, T. L., Baldwin, M. A., Cohen, F. E., James, T. L., and Prusiner, S. B. (1995) *J. Mol. Biol. 250*, 514−526.
17. Jackson, G. S., Hosszu, L. L. P., Power, A., Hill, A. F., Kenney, J., Saibil, H., Craven, C. J., Waltho, J. P., Clarke, A. R., and Collinge, J. (1999) *Science 283*, 1935−1937.
18. Zhang, H., Stöckel, J., Mehlhorn, I., Groth, D., Baldwin, M. A., Prusiner, S. B., James, T. L., and Cohen, F. E. (1997) *Biochemistry 36*, 3543−3553.
19. Brown, D. R., Qin, K., Herms, J. W., Madlung, A., Manson, J., Strome, R., Fraser, P. E., Kruck, T., von Bohlen, A., Schulz-Schaeffer, W., Giese, A., Westaway, D., and Kretzschmar, H. (1997) *Nature 390*, 684−687.
20. Hornshaw, M. P., McDermott, J. R., Candy, J. M., and Lakey, J. H. (1995) *Biochem. Biophys. Res. Commun. 214*, 993−999.
21. Stöckel, J., Safar, J., Wallace, A. C., Cohen, F. E., and Prusiner, S. B. (1998) *Biochemistry 37*, 7185−7193.
22. Muramoto, T., Scott, M., Cohen, F. E., and Prusiner, S. B. (1996) *Proc. Natl. Acad. Sci. U.S.A. 93*, 15457−15462.

23. Lee, C. H., Moseley, S. L., Moon, H. W., Whipp, S. C., Gyles, C. L., and So, M. (1983) *Infect. Immun. 42*, 264−268.
24. Picken, R. N., Mazaitis, A. J., Mass, W. K., Rey, M., and Heyneker, H. (1983) *Infect. Immun. 42*, 269−275.
25. Mehlhorn, I., Groth, D., Stöckel, J., Moffat, B., Reilly, D., Yansura, D., Willett, W. S., Baldwin, M., Fletterick, R., Cohen, F. E., Vandlen, R., Henner, D., and Prusiner, S. B. (1996) *Biochemistry 35*, 5528−5537.
26. Sreerama, N., and Woody, R. W. (1993) *Anal. Biochem. 209*, 32−44.
27. Uversky, V. N. (1993) *Biochemistry 32*, 13288−13298.
28. Baskakov, I. V., and Bolen, D. W. (1998) *Biochemistry 37*, 18010−18017.
29. Hilser, V. J., and Freire, E. (1995) *Anal. Biochem. 224*, 465−485.
30. Hornemann, S., and Glockshuber, R. (1998) *Proc. Natl. Acad. Sci. U.S.A. 95*, 6010−6014.
31. Swietnicki, W., Petersen, R., Gambetti, P., and Surewicz, W. K. (1997) *J. Biol. Chem. 272*, 27517−27520.
32. Bamborough, P., Wille, H., Telling, G. C., Yehiely, F., Prusiner, S. B., and Cohen, F. E. (1996) *Cold Spring Harbor Symp. Quant. Biol. 61*, 495−509.
33. Harper, J. D., and Lansbury, P. T., Jr. (1997) *Annu. Rev. Biochem. 66*, 385−407.
34. Cohen, F. E., and Prusiner, S. B. (1998) *Annu. Rev. Biochem. 67*, 793−819.
35. Jarrett, J. T., and Lansbury, P. T., Jr. (1993) *Cell 73*, 1055−1058.
36. Carlson, G. A., Ebeling, C., Yang, S.-L., Telling, G., Torchia, M., Groth, D., Westaway, D., DeArmond, S. J., and Prusiner, S. B. (1994) *Proc. Natl. Acad. Sci. U.S.A. 91*, 5690−5694.
37. Prusiner, S. B., Scott, M., Foster, D., Pan, K.-M., Groth, D., Mirenda, C., Torchia, M., Yang, S.-L., Serban, D., Carlson, G. A., Hoppe, P. C., Westaway, D., and DeArmond, S. J. (1990) *Cell 63*, 673−686.
38. Gajdusek, D. C. (1988) *J. Neuroimmunol. 20*, 95−110.
39. Terzi, E., Holzemann, G., and Seelig, J. (1995) *J. Mol. Biol. 252*, 633−642.
40. Chiti, F., Webster, P., Taddei, N., Clark, A., Stefani, M., Ramponi, G., and Dobson, C. M. (1999) *Proc. Natl. Acad. Sci. U.S.A. 96*, 3590−3594.
41. Guijarro, J. I., Sunde, M., Jones, J. A., Campbell, I. D., and Dobson, C. M. (1998) *Proc. Natl. Acad. Sci. U.S.A. 95*, 4224−4228.
42. Bessen, R. A., and Marsh, R. F. (1992) *J. Virol. 66*, 2096−2101.
43. Pan, K.-M., Baldwin, M., Nguyen, J., Gasset, M., Serban, A., Groth, D., Mehlhorn, I., Huang, Z., Fletterick, R. J., Cohen, F. E., and Prusiner, S. B. (1993) *Proc. Natl. Acad. Sci. U.S.A. 90*, 10962−10966.
44. Safar, J., Wille, H., Itri, V., Groth, D., Serban, H., Torchia, M., Cohen, F. E., and Prusiner, S. B. (1998) *Nat. Med. 4*, 1157−1165.
45. Telling, G. C., Parchi, P., DeArmond, S. J., Cortelli, P., Montagna, P., Gabizon, R., Mastrianni, J., Lugaresi, E., Gambetti, P., and Prusiner, S. B. (1996) *Science 274*, 2079−2082.
46. Wadsworth, J. D. F., Hill, A. F., Joiner, S., Jackson, G. S., Clarke, A. R., and Collinge, J. (1999) *Nat. Cell Biol. 1*, 55−59.

BI9923353